NANO LETTERS
Letter
Cite This: Nano Lett. 2017, 17, 6644-6652
pubs.acs.org/NanoLett

Longitudinal Monitoring of Antibody Responses against Tumor Cells Using Magneto-nanosensors with a Nanoliter of Blood

Jung-Rok Lee,[†,‡,◆] Carmel T. Chan,[§,◆] Daniel Ruderman,[∥] Hui-Yen Chuang,[§] Richard S. Gaster,[⊥,#] Michelle Atallah,[¶] Parag Mallick,[§] Scott W. Lowe,[▽] Sanjiv S. Gambhir,[§] and Shan X. Wang[*,‡,§,○]

[†]Division of Mechanical and Biomedical Engineering, Ewha Womans University, Seoul 03760, South Korea
[‡]Department of Materials Science and Engineering, Stanford University, Stanford, California 94305, United States
[§]Department of Medicine, Department of Radiology, Stanford University, Stanford, California 94305, United States
[∥]Ellison Institute of Transformative Medicine of USC, USC Keck School of Medicine, Los Angeles, California 90211, United States
[⊥]Department of Bioengineering, Stanford University, Stanford, California 94305, United States
[#]Pliant Therapeutics, Redwood City, California 94063, United States
[¶]Cancer Biology Program, Stanford School of Medicine, Stanford, California 94305, United States
[▽]Cancer Biology and Genetics Program, Memorial Sloan Kettering Cancer Center, New York, New York 10065, United States
[○]Department of Electrical Engineering, Stanford University, Stanford, California 94305, United States

Supporting Information

ABSTRACT: Each immunoglobulin isotype has unique immune effector functions. The contribution of these functions in the elimination of pathogens and tumors can be determined by monitoring quantitative temporal changes in isotype levels. Here, we developed a novel technique using magneto-nanosensors based on the effect of giant magneto-resistance (GMR) for longitudinal monitoring of total and antigen-specific isotype levels with high precision, using as little as 1 nL of serum. Combining *in vitro* serologic measurements with *in vivo* imaging techniques, we investigated the role of the antibody response in the regression of firefly luciferase (FL)-labeled lymphoma cells in spleen, kidney, and lymph nodes in a syngeneic Burkitt's lymphoma mouse model. Regression status was determined by whole body bioluminescent imaging (BLI). The magneto-nanosensors revealed that anti-FL IgG2a and total IgG2a were elevated and sustained in regression mice compared to non-regression mice ($p < 0.05$). This platform shows promise for monitoring immunotherapy, vaccination, and autoimmunity.

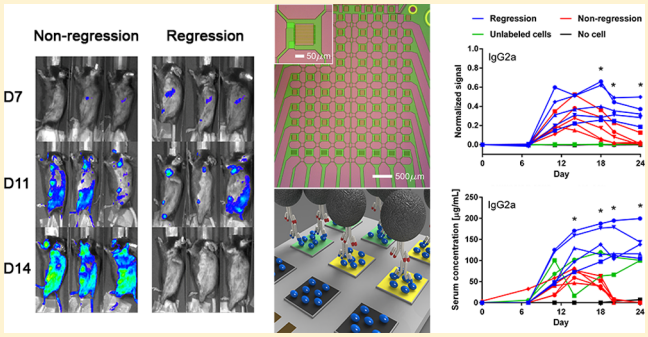

KEYWORDS: *Magneto-nanosensors, bioluminescent imaging, magnetic nanoparticles, lymphoma, cancer immunology, immunoglobulin isotypes*

Serum antibody levels are routinely measured to assess an individual's immune status, including vaccination status and disease diagnosis,[1−3] because they reflect the humoral immune response to certain types of pathogens. For example, the existence of circulating antibodies against human immunodeficiency virus (HIV) and hepatitis B virus (HBV) may reveal the individual's infection history or current status associated with each pathogen. Furthermore, serum antibody response against tumor-associated antigens (TAAs) could indicate which antitumor immune effector functions are activated. However, although antibody-based therapy against tumors has been successfully implemented to trigger antitumor immune response,[4,5] the role of humoral immunity in the antitumor immune response remains unclear.[6] To facilitate immunization tests, disease diagnostics, and antitumor immunity studies, various methods have been developed to measure serum antibodies. Recently, microarray techniques enabled multiplexed serum measurements by combining different assays into a single platform for detection of autoantibodies in autoimmune diseases,[7,8] screening of autoantibodies in cancer,[9] and estimation of vaccination efficacy.[10,11] Although an antibody microarray test can reveal immunity against multiple targets, its limitations include that it is still a snapshot of immune status at the time point of test and that it is difficult to accurately measure multiple time-point samples with different arrays due to array-to-array variations. Even though multiple samples are allocated on a single array, fluorescence-based planar microarrays require

Received: June 19, 2017
Revised: September 12, 2017
Published: October 9, 2017

DOI: 10.1021/acs.nanolett.7b02591
Nano Lett. 2017, 17, 6644−6652

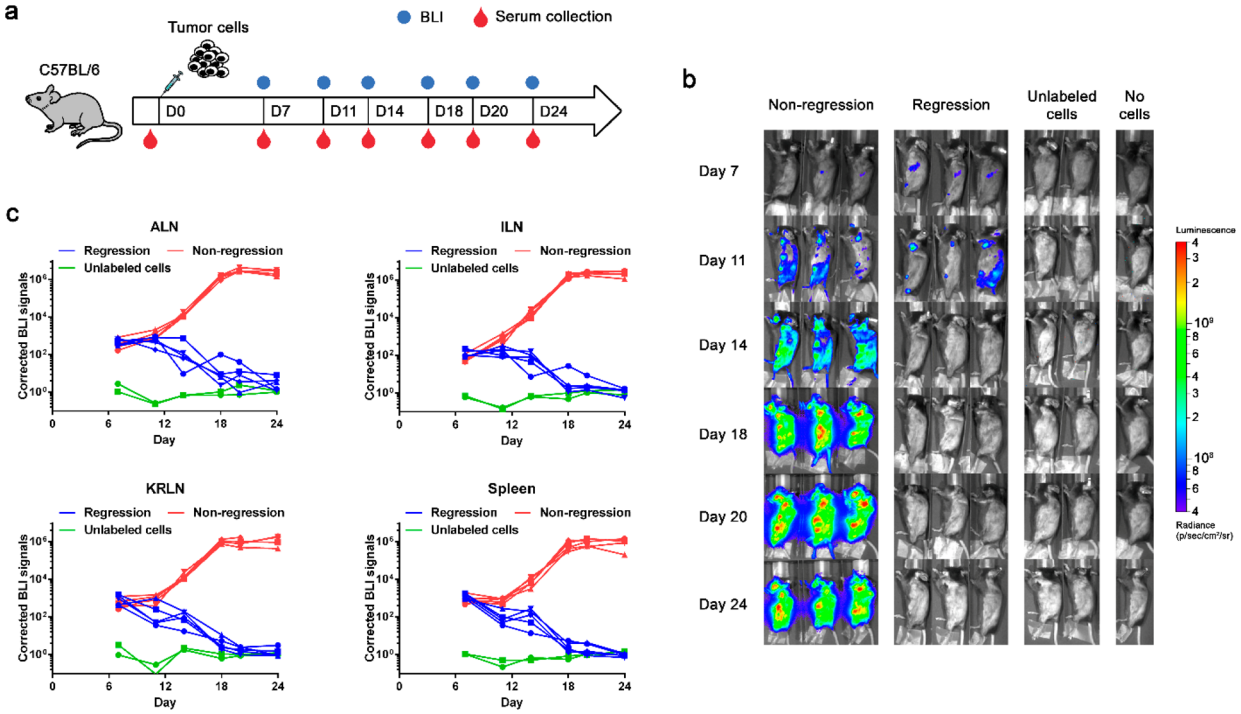

Figure 1. Live mouse BL imaging of tumor regression. (a) Schematic of BLI coupled with serum antibody measurement by magneto-nanosensors. Arf null lymphoma cells were labeled with a FL−eGFP fusion reporter prior to injection into syngeneic C57BL/6 mice. Whole body BLI and blood draw (20 μL) were performed at different time points post-cell-injection in mice. (b) Representative images of mouse groups. Decrease in BLI signals in mice that exhibit lymphoma regression was observed, compared to those of non-regression mice. Mice injected with an equal number of unlabeled Arf null lymphoma cells or with HBSS served as negative controls. (c) BLI signals (average radiance over area) at different time points post-cell-injection in spleen, ALN, ILN, and kidney with renal lymph nodes (KRLN) subtracted from control mice without any cell injection. The BLI signals in spleen and lymph nodes decreased dramatically in regression mice compared to those of non-regression mice starting on day 14. All non-regression mice died on day 24 post-cell-injection.

normalization of signals and variations of spot sizes that produce high uncertainty in quantitative measurement.[7,12,13] In addition, recent studies have focused more on the importance of individual antibody isotypes in meditating immune responses,[14,15] instead of overall reactivity of antibodies to certain targets because each isotype has different effector functions and temporal expression. This measurement of isotypes provides a more informative picture of which pathways are activated and how the immune system interacts with the targets.

Bioluminescent imaging (BLI) enables noninvasive longitudinal tracking of firefly luciferase (FL)-labeled cells within living mice.[16] Spontaneous tumor regression has been observed in syngeneic immunocompetent mice that were injected with FL-labeled tumor cells,[17] and we have found that about 16% of mice showed spontaneous regression after being transplanted with Burkitt's lymphoma cells, as determined by BLI and confirmed by caliper measurements. Lymphoma is a systemic disease, and FL is a foreign protein that can be targeted by the immune system. These features allowed us to use a mouse lymphoma model to demonstrate the capability of magneto-nanosensors to monitor longitudinal global antibody responses in terms of its isotypes by combining *in vitro* magneto-nanosensor technique with *in vivo* site-specific BLI. Previously, the magneto-nanosensor chips were demonstrated to be a promising transformative proteomics platform with femtomolar range sensitivity, because they are matrix- and temperature-insensitive due to use of magnetic nanoparticles (MNPs)[18−20] and employment of advanced signal processing schemes that enable fast readout and multiplexing capability.[21] Here we describe a new method for longitudinally monitoring antigen-specific and total isotypes of IgG in serum using a significantly smaller sample volume for the magneto-nanosensors. The *in vitro* measurement was coupled with *in vivo* BLI of FL-labeled lymphoma cells in a syngeneic immunocompetent mouse model. The quantitative detection of both IgG isotypes allowed us to systemically understand the interactions between the host (immune system) and tumors and analyze which pathway(s) of the immune system was being activated to eliminate the tumors.

To generate a tumor mouse model for this study, we injected 0.3 million Eμ-myc/Arf null mouse lymphoma cells[22] labeled with a FL−eGFP fusion reporter into syngeneic female C57BL/6 mice via tail vein and monitored their growth at the lymph nodes (renal, RLN; inguinal, ILN; and axillary, ALN), kidney, and spleen by BLI. As a negative control, we injected 0.3 million non-FL expressing Eμ-myc/Arf null mouse lymphoma cells into another set of mice (n = 3). To determine the background BLI signals due to substrate (D-luciferin), mice (n = 2) were injected with the vehicle (Hank's Balanced Salt Solution, HBSS). Bioluminescence images were taken twice a week for each mouse starting 7 days after the cell injections. Serum samples were collected on the same days as BLI, and prior to cell injections to establish the baseline of antibody responses (Figure 1a). Tumor volume measurements of the ALN and ILN were performed starting on day 11, when palpable. Based on BLI measurements for the first 24 days, 5 mice were classified as regression mice and another 5 mice were classified as non-regression mice for subsequent analyses. Figure 1b shows the bioluminescent images of representative mice in each experimental group. The regression of tumor cells in the 5 mice was also confirmed with ALN and ILN tumor volume measurement

DOI: 10.1021/acs.nanolett.7b02591
Nano Lett. 2017, 17, 6644−6652

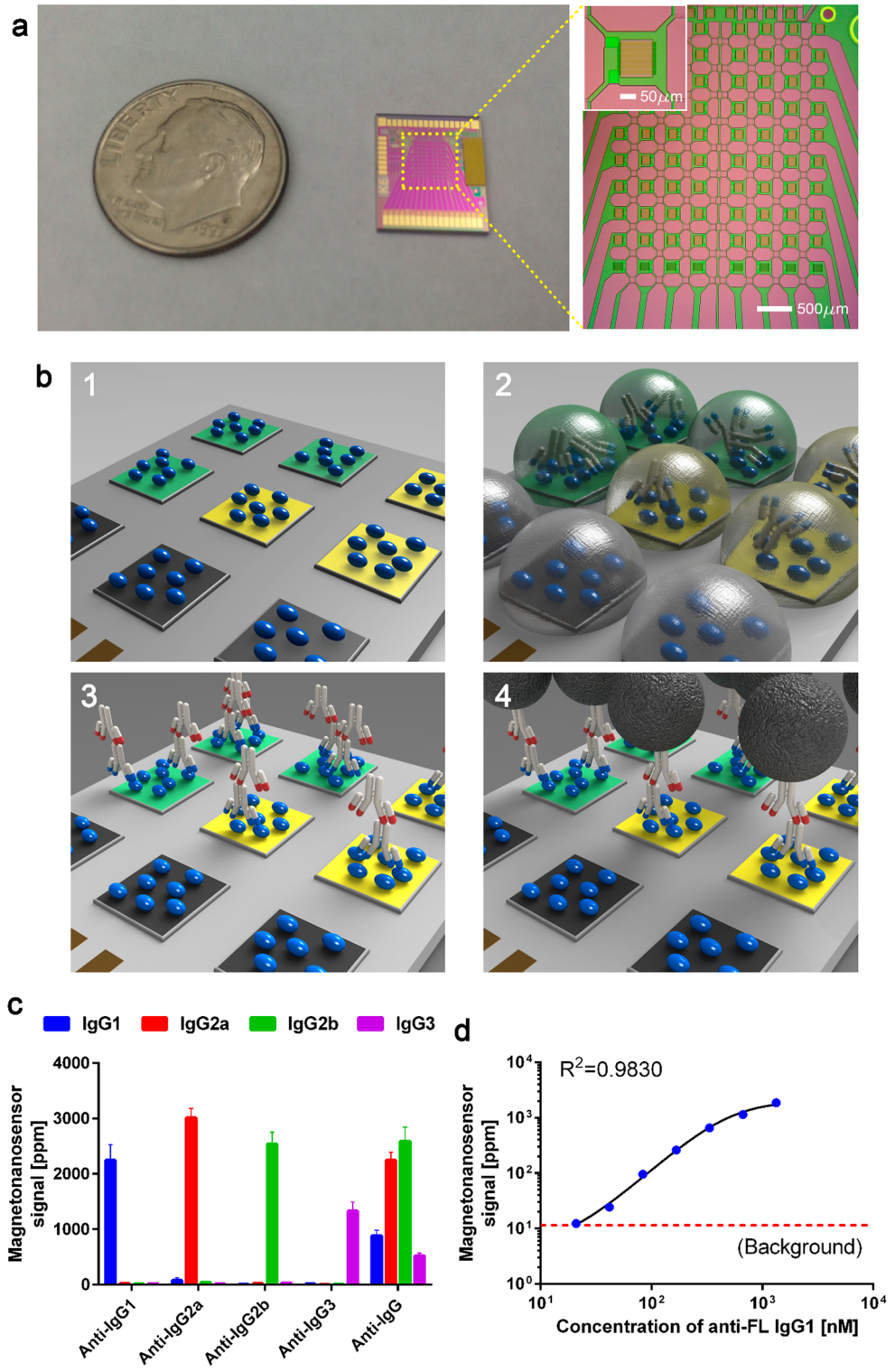

Figure 2. Development of antigen-specific isotype assays. (a) Left, image of magneto-nanosensor chip with a dimension of 10 mm × 12 mm and US dime (17.9 mm diameter). Right, individually accessible 8 × 10 sensor array on a chip. Inset, sensor element with a dimension of 100 μm × 100 μm. (b) Schematic of the assay (not to scale). (1) FL (blue ovals) was immobilized on the sensors. (2) Multiple serum samples taken at different time points were deposited on sensors coated with FL by a noncontact arrayer. The volume of the sample on a sensor is about 1 nL. Green represents the sensors with samples containing a higher concentration of anti-FL antibodies (antibody with blue tips), and yellow represents the sensors with samples that have a lower concentration of anti-FL antibodies. Black represents the sensors without anti-FL antibody. If anti-FL antibodies exist in the samples, they will bind to the FL on the sensors. (3) After washing the chip, isotype-specific secondary antibodies (antibody with red tips) were added. (4) MNPs bound to the secondary antibodies via biotin−streptavidin interaction. The magnetic field from the MNPs can be detected by the magneto-nanosensor underneath under an externally applied magnetic field. (c) Specificities of isotype-specific secondary antibodies. Each group of sensors was functionalized with different purified mouse IgG isotypes (IgG1, IgG2a, IgG2b, and IgG3) in a different set of sensor chips, and one type of isotype-specific secondary antibodies (anti-IgG1, anti-IgG2a, anti-IgG2b, or anti-IgG3) was added to each chip. The MNPs were then introduced to label the secondary antibodies to determine the reactivity of the antibody to the isotypes. Each secondary antibody was highly specific to its targeted isotype (Max

DOI: 10.1021/acs.nanolett.7b02591
Nano Lett. 2017, 17, 6644−6652

Figure 2. continued

cross-reactivity = 2.6%), and anti-IgG secondary antibodies should bind to all isotypes. (d) Titration curve of anti-FL IgG1 detection using magneto-nanosensors. Serial dilution (2-fold) samples were measured, and 4 parameter logistic (4PL) nonlinear regression model was used for the curve fitting (black solid line, $R^2 = 0.9830$). The background level (red dashed line) was determined by the average signal of zero concentration of the antibody and two standard deviations. The detection limit is 20 nM.

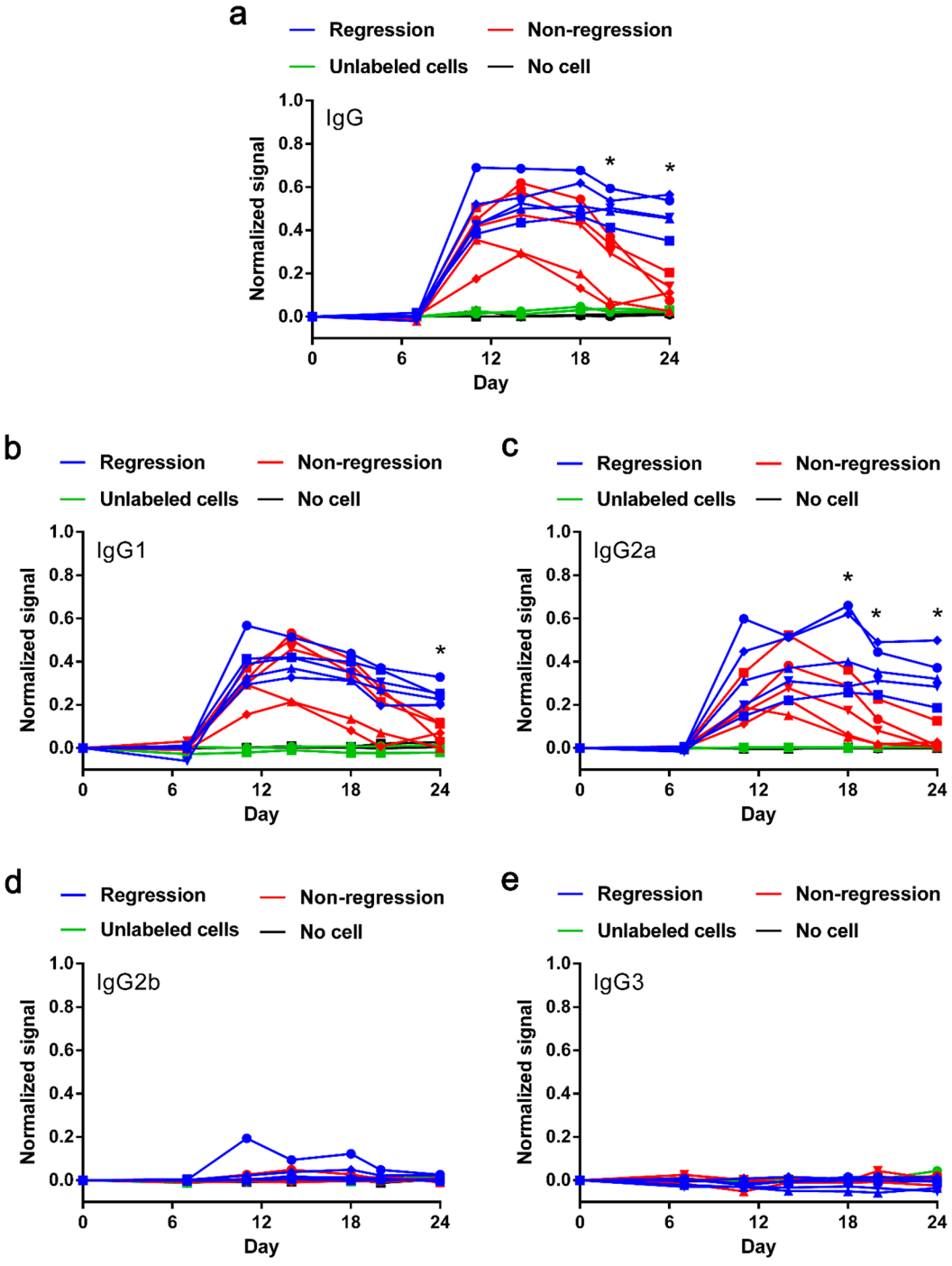

Figure 3. Profiles of anti-FL IgG isotypes measured by magneto-nanosensors. The serum samples from regression (blue, $n = 5$), non-regression (red, $n = 5$), unlabeled cell injected (green, $n = 2$), and no cell injected (black, $n = 2$) mice were measured for each isotype against FL. Each data point is the average signal of triplicates, and the baseline signals (day 0) were subtracted from all later time point signals to easily compare the differences. The signals were further normalized by the maximum detection signal. Different symbols on the connected lines indicate different mice. A statistical test (t-test) was performed at each time point between regression and non-regression groups, and the data point is denoted with an asterisk if $p < 0.05$ and false discovery rate (FDR) < 10%: (a) Anti-FL IgG. (b) Anti-FL IgG1. (c) Anti-FL IgG2a. (d) Anti-FL IgG2b. (e) Anti-FL IgG3.

DOI: 10.1021/acs.nanolett.7b02591
Nano Lett. 2017, 17, 6644−6652

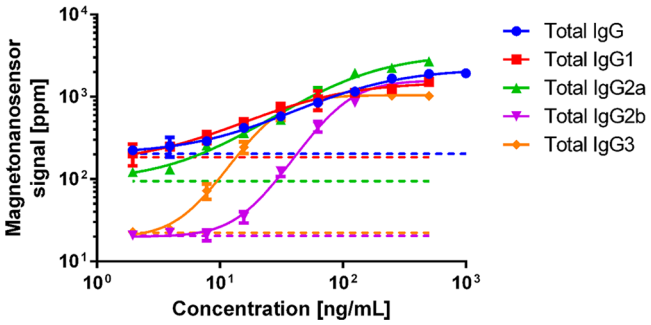

Figure 4. Titration curves of total isotype detection with magneto-nanosensors. Two-fold serial dilution samples of each isotype were measured, and 4 parameter logistic (4PL) nonlinear regression models were used for the curve fitting (solid lines, IgG, $R^2 = 0.9961$; IgG1, $R^2 = 0.9931$; IgG2a, $R^2 = 0.9775$; IgG2b, $R^2 = 0.9835$; and IgG3, $R^2 = 0.9938$). The background levels (dashed lines with the same color codes) were determined by the average signal of zero isotype measurement and two standard deviations.

by caliper (Figure S1). In addition, we found that the BLI signals were well correlated with the number of labeled lymphoma cells at all sites measured. Figure 1c indicates that the decreases in area-averaged BLI signals at ALN, ILN, and kidney with RLN (KRLN), as well as spleen, have similar regression patterns, even though we observed slightly early decrease of the signals in spleen of the regression mice.

To detect antibodies in serum samples, we developed a novel technique to measure multiple serum samples with a single magneto-nanosensor chip. This technique requires about 10 nL of sample to measure all antigen-specific and total isotypes together, which allows us to longitudinally study the presence of FL antibodies (IgG and IgG1/IgG2a/IgG2b/IgG3) in the same mice with bleeding at each imaging time point. In contrast, conventional ELISA usually requires 50−100 μL serum samples to measure only one parameter among them, which requires at least 1 mL of bleeding for 10 parameters (anti-FL and total isotypes, see Figure S2). Magneto-nanosensors can measure all the isotypes (5 antigen-specific and 5 total) using only 10 nL of serum (1 nL per each parameter to cover the active sensing area of a magneto-nanosensor). Each chip consists of 72 sensor elements that can be individually functionalized with target proteins or antibodies (capture probes) to detect serum antibodies or other analyte of interest (Figure 2a). Each sample is delivered separately to designated sensors using a noncontact arrayer. The serum antibodies bound to the capture probes are labeled with isotype-specific biotinylated secondary antibodies that subsequently bind to streptavidin-coated MNPs (Figure 2b). The magneto-nanosensor underneath these sandwich complexes can detect stray magnetic fields from the MNPs and produce electrical signals proportional to the number of the MNPs.[23] Once plateaued, the signals are taken for the further analyses (Figure S3). This measurement takes less than 20 min. To differentiate each isotype of serum antibodies, the secondary antibodies should be highly specific to their target isotypes. Thus, monoclonal secondary antibodies were screened with the sensor chips that contain purified mouse IgG1, IgG2a, IgG2b, and IgG3-coated sensors to check for cross-reactivity of the secondary antibodies with different isotypes (Figure 2c and Figure S4), and the maximum cross-reactivity between isotypes was 2.6%. To validate the technique, commercial anti-FL IgG1 was prepared at different concentrations (21−1333 nM), and deposited on FL-coated sensors separately. As shown in Figure 2d, the assay has a wide and linear range of detection (in a log−log plot), and it enables quantification of the number of antibodies bound to the sensors. In regard to the detection limit, the antibodies at a few nanomolar concentration in 1 nL corresponds to several hundreds of thousands of the antibodies. Due to the affinity between the antibodies and capture probes, not every single antibody molecule will bind to the capture probes at equilibrium. Thus, we believe that several tens of thousands or fewer antibodies are actually binding to the surface of a sensor at the limit of detection, and it is close to the intrinsic sensitivity of the magneto-nanosensor. The advantage of using a sensor array is a low intrachip variation (less than 10%), which enables accurate relative measurement of multiple samples on a single chip in a single assay. The signals from the magneto-nanosensors are confined by the actual size of the sensor element (100 μm × 100 μm, shown in Figure 2a) when the sample covers the actual sensor area (0.01 mm^2). This is because the magneto-nanosensors can only detect the MNPs in their immediate proximity (within 150 nm).[24,25] Due to the nanoscale precision photolithography sensor fabrication technique, the size of sensor elements on a chip is highly reproducible, even across different chips. Furthermore, it is feasible to generate sample spots large enough to cover the entire area of sensor element using a noncontact arrayer. These features enable a high accuracy measurement across multiple samples on a single chip.

To determine whether the immune response plays a key role in the regression of FL-labeled lymphoma cells in syngeneic mice, we measured the serum samples from the same cohort where the BLI signals were monitored. IgG2a is known to be more effective in triggering antibody-dependent cell-mediated cytotoxicity (ADCC) via higher binding affinities to the Fc receptors, compared to other isotypes, in elimination of tumor cells.[14,26,27] In a similar manner to detecting the commercial anti-FL IgG1 antibody, FL was immobilized on the sensors and all samples (0, 7, 11, 14, 18, 20, and 24 days post-cell-injections) from each of two mice were deposited on the different sensors, in triplicate per chip. A prealiquoted and frozen mouse serum sample from a regression mouse showing a detectable level of anti-FL antibodies (IgG and its isotype) from a separate cohort was also deposited on each chip. The signals from these sensors were used to normalize the serum antibody signals across the chips, that is, across different mice, isotypes, and days of the measurement. Five chips with the same sample pattern were prepared and probed with different isotype-specific secondary antibodies (anti-IgG, anti-IgG1, anti-IgG2a, anti-IgG2b, and anti-IgG3) (Figure S5). To measure serum samples from all mice, the entire procedure was repeated 7 times with different sets of samples. The order of measurement and preparation, physical locations of samples on the sensors, and reader stations were all randomized to reduce possible bias from the order of sample deposition, variation in fabrication, and location of the sensors within each chip. We found that only the order of sample deposition affected the signals (Figure S6a). However, it was confirmed by comparing statistical tests before and after correction that this factor did not significantly change our findings (Figure S6b). After normalization of signals using the common sample, each isotype signal was further divided by the maximum signal that can be produced by the each sensor chip. No significant antibody was detected until 7 days post-cell-injection, but a substantial amount of IgG against FL was found in the serum samples of both regression (n = 5) and non-regression (n = 5) mice starting on day 11 (Figure 3a). Since both anti-FL IgG1 and IgG2a in the non-regression mice decreased

DOI: 10.1021/acs.nanolett.7b02591
Nano Lett. 2017, 17, 6644−6652

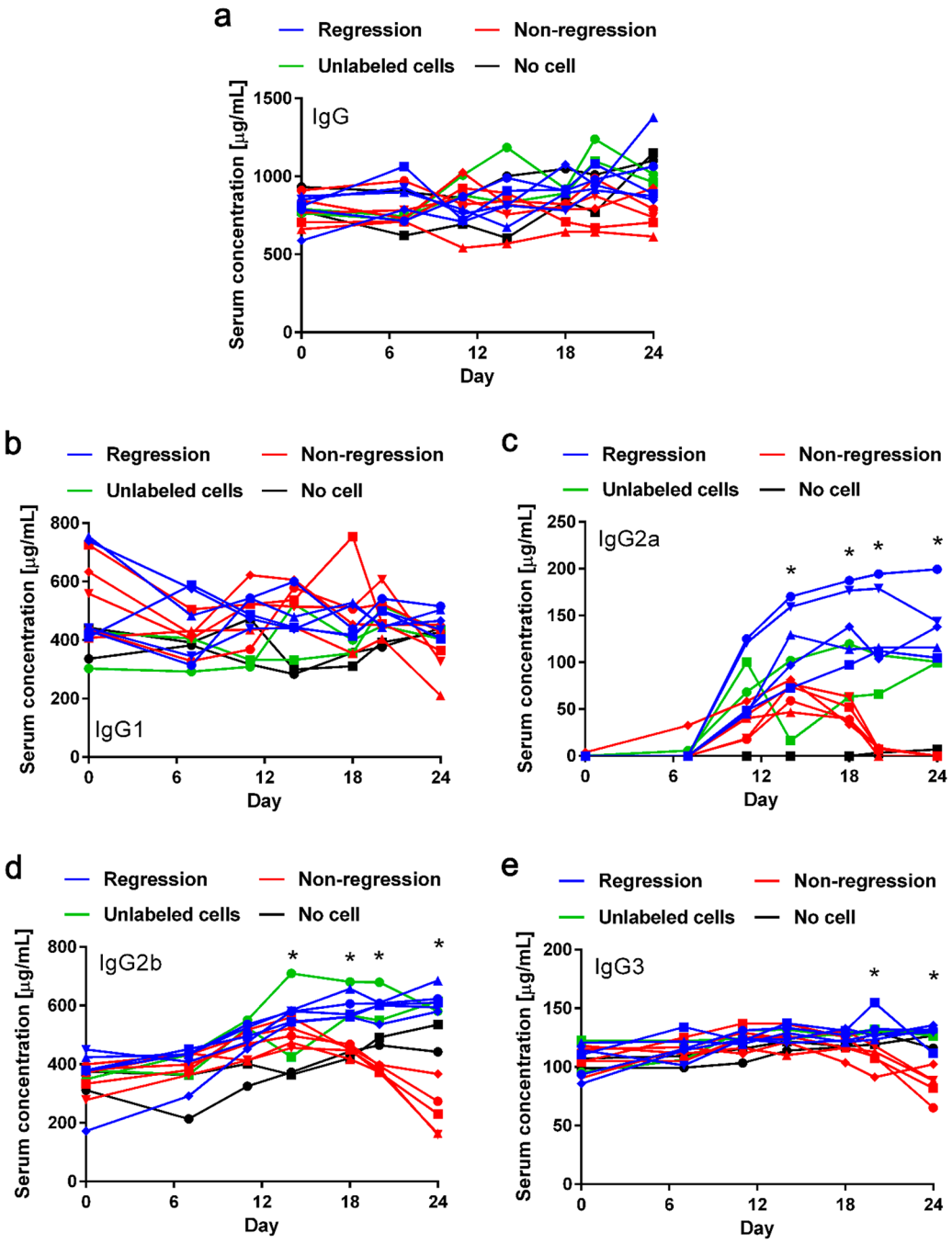

Figure 5. Profiles of total IgG isotypes measured by magneto-nanosensors. The serum samples from regression (blue, $n = 5$), non-regression (red, $n = 5$), unlabeled cell injected (green, $n = 2$), and no cell injected (black, $n = 2$) mice were measured for the total concentration of each isotype (including FL and non-FL specific). Each data point is the average signal of triplicates, and the signals were converted into the serum concentrations using the titration curves. Different symbols on the connected lines indicate different mice. A statistical test (t-test) was performed at each time point between regression and non-regression groups, and the data point is denoted with an asterisk if $p < 0.05$ and false discovery rate (FDR) < 10%. (a) Total IgG. (b) Total IgG1. (c) Total IgG2a. (d) Total IgG2b. (e) Total IgG3.

faster than those in the regression mice (Figure 3b,c, Table S1 for all p-values), the IgG response dropped more rapidly in the non-regression mice. Notably, the levels of anti-FL IgG2a in regression mice were maintained relatively constant after their onsets and showed statistically significant difference ($p < 0.05$) 18 days after the cell injection, earlier than anti-FL IgG. No significant levels of anti-FL IgG2b and IgG3 were detected for the duration of the study (Figure 3d,e). Furthermore, mice injected with non-FL-expressing lymphoma cells or with the vehicle (HBSS) showed no significant antibody signals during the course of time ($p > 0.05$ in all cases), further demonstrating the specificity of the magneto-nanosensors.

To measure the total concentration of each isotype (including both FL and non-FL specific antibodies), isotype-specific capture antibodies were immobilized on another set of the sensor chips in lieu of FL (Figure S7). The samples were deposited on the sensors using the same arrangement (Figure S8), and the same isotype-specific secondary antibodies were used. Unlike the case of antigen-specific isotype detection, where only anti-FL IgG1 is commercially available (Figure 2d), all total isotypes are

DOI: 10.1021/acs.nanolett.7b02591
Nano Lett. 2017, 17, 6644−6652

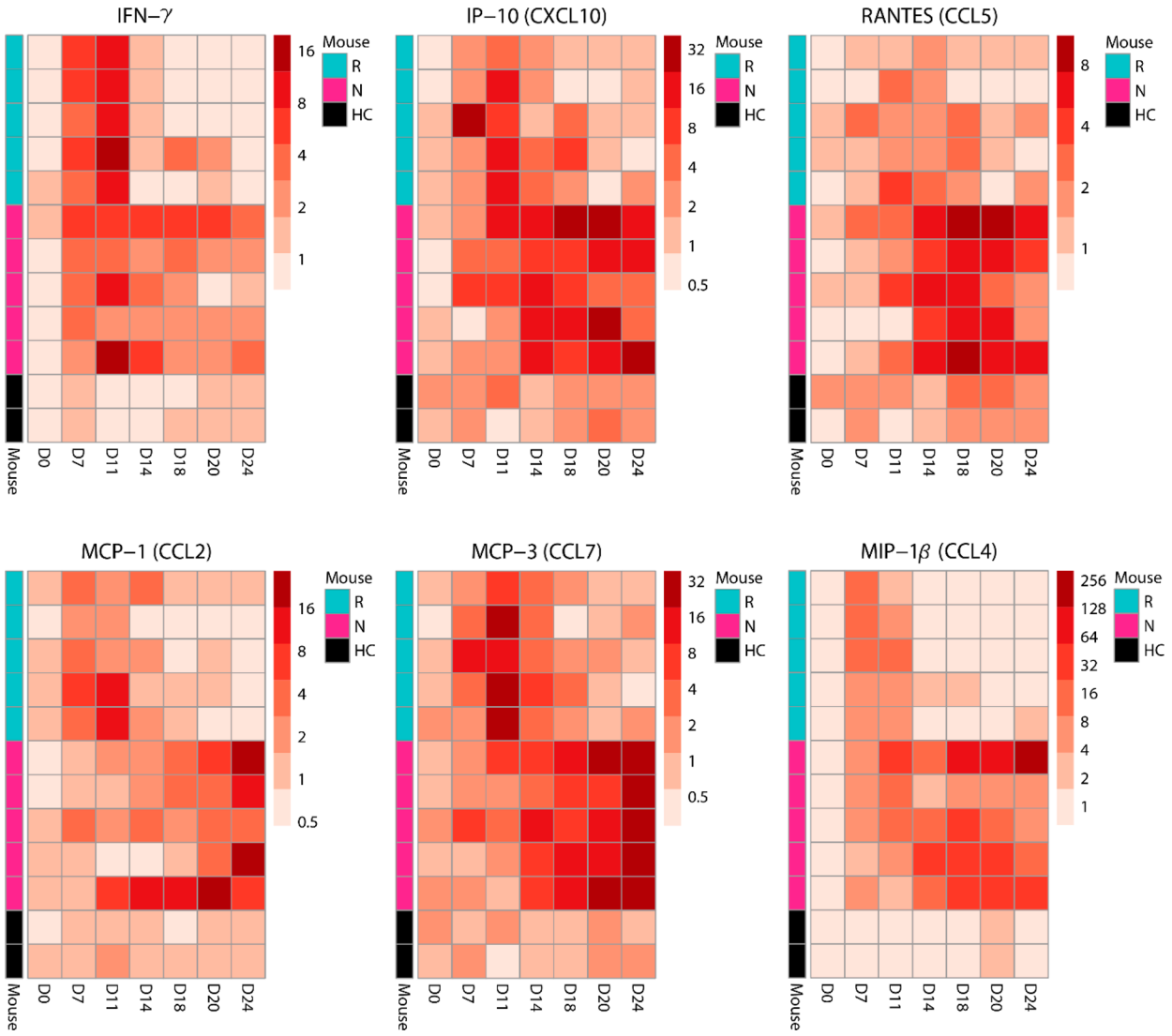

Figure 6. Levels of serum IFN-γ and inducible chemokines. The serum samples from regression (denoted as R in blue, $n = 5$), non-regression (denoted as N in red, $n = 5$), no cell injected (denoted as HC in black, $n = 2$) mice were processed for bead-based cytokine and chemokine measurement. The MFI normalized by the signal of day 0 for each mouse was plotted in log scale. The peak of IFN-γ was observed on day 11 in the regression mice, which is well correlated with onset of antibody response. IFN-inducible chemokines (IP-10, RANTES, MCP-1, MCP-3, and MIP-1β) showed similar patterns.

commercially available. Thus, each isotype (IgG 2−1000 μg/mL, and others 2−500 μg/mL) was titrated on different chips as standard curves (Figure 4). In addition, the same normalization and randomization schemes were applied to the measurement. Based on the measurement of the common sample across the chips, the variations between chips and measurement days were calculated, giving a maximum interchip coefficient of variation (CV) of 17.6%. This variation was corrected through normalization by the common sample. Since all measured signals were within the dynamic ranges of the standard curves, excluding data points below the detection limit, the signals were converted into the concentrations. Total concentrations of mouse IgG in all mice were maintained constant over time (Figure 5a) because the predominant isotype, IgG1,[14] remained the same during the course of the experiment (Figure 5b). Interestingly, the levels of total IgG2a were initially low, and became detectable starting 11 days after the injection of the tumor cells (Figure 5c). Similar to FL-specific IgG2a, the total IgG2a levels remained constant in the regression mice, while they decreased after the onset in the non-regression mice after day 11 ($p < 0.05$), which is again earlier than the total IgG. The concentration of IgG2a in the regression mice was approximately 2 times higher than that in the non-regression mice after day 11 (Table S2). Interestingly, total IgG2a levels in the mice with unlabeled cells are similar to those in the regression mice. The ILN and ALN tumor volume measurements showed that the tumors regressed in these mice as well (Figure S1). This can indicate that the total IgG2a is a key isotype involved with eliminating the tumor cells. The levels of total IgG2b and IgG3 were dropping at the later time points only in the non-regression mice, while those in the regression mice remain stably elevated (Figure 5d,e). In addition, since the anti-IgG secondary antibodies used for total IgG measurement do not have the same affinity to each isotype as isotype-specific monoclonal secondary antibodies (Figure 2c), the measured concentrations of total IgG1, IgG2a, IgG2b, and IgG3 did not add up to the measured concentration of total IgG. Once the reactivity of secondary antibodies was corrected, the signals were well-matched (Figure S9). Moreover, the substantial increases in total IgG2a did not clearly appear in the total IgG, because the majority of IgG was IgG1 and IgG2b (Figure 5b,d).

DOI: 10.1021/acs.nanolett.7b02591
Nano Lett. 2017, 17, 6644−6652

It has been reported that the IgG2a signature is one of the characteristics of T helper 1 (T_H1) cell-mediated immunity, whereas T helper 2 (T_H2) cells promote IgG1.[28] In addition, since T_H1 and T_H2 cells are differentially regulated,[29] the decreasing levels of anti-FL IgG1 and sustaining levels of anti-FL IgG2a are indicative of an immune response shifted from T_H2 cell-mediated to T_H1 cell-mediated immunity. To support that T_H1 cells were involved with the regression, serum cytokines and chemokines were measured with 38-plex bead-based assays because T_H1 cells are known to secrete IFN-γ, while T_H2 cells produce mainly IL-4.[30] The signals of mean fluorescent intensity (MFI) were normalized by the average of all day 0 signals for each cytokine and plotted for each mouse. The levels of IFN-γ started increasing on day 7 and peaked on day 11 in the regression mice and dropped back to the initial levels (before tumor injection). In the non-regression mice, however, their levels were sustained at the elevated levels from day 0 (Figure 6). Furthermore, IFN-inducible chemokines such as IP-10 (CXCL10), RANTES (CCL5), MCP-1 (CCL2), MCP-3 (CCL7), and MIP-1β (CCL4) had similar patterns to the IFN signature. We also observed that the levels of GCSF, IL-6, and TNF-α resembled those of IFN-γ and its related chemokines. We detected no significant change in IL-4 (Figure S10).

Using a mouse tumor model combined with BLI, we have demonstrated that magneto-nanosensors are capable of longitudinal monitoring of antibody response, including antigen-specific and total isotypes of IgG. Using this technique, we observed that the levels of anti-FL and total IgG2a remain high in tumor-regression mice ($p < 0.05$) 14 days after injection with FL-labeled mouse lymphoma cells. Conventional IgG measurement without isotyping would have missed this effect, validating the importance of this technique. Additionally, the IFN-γ signature was observed on day 11, in accordance with onset of IgG2a. We believe that T_H1 cell-mediated immunity became prevalent and that it may have played a key role in eliminating tumor cells in the regression mice.

We anticipate this technique can be further used to study immunotherapy, detect autoantibodies in cancer and autoimmune diseases, and estimate efficacy of vaccinations. Dendritic cell-based and T cell-based immunotherapies have been studied over the past several decades.[31,32] However, the antibody response against targets induced by the immunotherapy has not been well studied.[6] This technique allows us to conduct research to determine the signature(s) of isotypes in regression after immunotherapy and the role of the humoral response in antitumor immunity. Recently, autoantibody signatures have been used for early cancer detection,[33] and autoantibody measurement has been a key component in the diagnosis of many autoimmune diseases.[19,34,35] Most current studies have focused on the signature of autoantibodies at the time of diagnosis, although the presence of autoantibodies has been shown to precede clinical onset of disease.[36] This technique could enable studying temporal changes in autoantibody levels in patients over the development of the disease. In addition to confirming immunization status of a patient, the magneto-nanosensors can provide a platform to study the time frame required to develop antibodies against vaccines, determine the isotype(s) involved in the vaccine response, and estimate the decay rates of the antibodies with high accuracy to administer a timely booster shot.

Since the magneto-nanosensor array is scalable,[37] we anticipate that the next generation of magneto-nanosensor chips will have a denser detection array that can be used to longitudinally monitor hundreds of samples simultaneously in a single chip. Given that this technique requires as little as 1 nL of a serum sample to measure one isotype, it can be easily implemented into point-of-care (POC) devices.[24,38] To miniaturize the device, a simple microfluidic chip or stamp method can be employed to deliver samples to designated sensors.[39] This strategy can help us evaluate individuals' immunization status rapidly and affordably with a drop of blood from a finger-prick or in combination with microneedle techniques.[40−42]

■ ASSOCIATED CONTENT

Supporting Information

The Supporting Information is available free of charge on the ACS Publications website at DOI: 10.1021/acs.nanolett.7b02591.

Methods, tumor volume measurement, isotypes of IgG, magneto-nanosensor signals, specificities of secondary antibodies, workflow of antigen-specific antibody measurement, effects of nuisance factors, statistical tests on isotype measurements, schematic of total isotype assays, workflow of total isotype measurement, quantitative fold-changes of total isotypes, corrected concentration measurements, and serum cytokine levels (PDF)

■ AUTHOR INFORMATION

Corresponding Author

*E-mail: sxwang@stanford.edu.

ORCID

Jung-Rok Lee: 0000-0002-3518-3965

Author Contributions

◆J.-R.L. and C.T.C. contributed equally. J.-R.L. designed experiments, developed and performed magneto-nanosensor assays, interpreted data, and prepared manuscript. C.T.C. designed experiments, conducted animal experiments, interpreted data, and prepared manuscript. D.R. analyzed data and performed randomization of the experiments. H.Y.C. assisted in mouse imaging and collection of sera. R.S.G. assisted in development of the assays. M.A. assisted in conducting animal experiments. P.M. provided guidance and assisted in manuscript preparation. S.W.L. provided cell lines and guidance on mouse model. S.S.G. provided guidance and assisted in manuscript preparation. S.X.W. supervised the project, provided guidance, and prepared manuscript.

Notes

The authors declare the following competing financial interest(s): R.S.G. and S.X.W. have related patents or patent applications assigned to Stanford University and out-licensed for potential commercialization. R.S.G. and S.X.W. have stock or stock options in MagArray, Inc., which has licensed relevant patents from Stanford University for commercialization of magneto-nanosensor chips.

■ ACKNOWLEDGMENTS

This work was supported by Physical Science Oncology Center (U54CA143907), Center for Cancer Nanotechnology Excellence (U54CA151459 and U54CA199075), and the Ewha Womans University Research Grant of 2017. We thank Dr. Cornelius Miething for providing the serum samples for the preliminary experiments and Drs. Masa Kotsuma and Ken Ito for their help with the preliminary tests of the assay.

DOI: 10.1021/acs.nanolett.7b02591
Nano Lett. 2017, 17, 6644−6652

REFERENCES

(1) Ghany, M. G.; Strader, D. B.; Thomas, D. L.; Seeff, L. B. *Hepatology* **2009**, *49* (4), 1335−1374.
(2) Reynolds, S. J.; Muwonga, J. *Expert Rev. Mol. Diagn.* **2004**, *4* (5), 587−91.
(3) Kavanaugh, A.; Tomar, R.; Reveille, J.; Solomon, D. H.; Homburger, H. A. *Arch Pathol Lab Med.* **2000**, *124* (1), 71−81.
(4) Scott, A. M.; Wolchok, J. D.; Old, L. J. *Nat. Rev. Cancer* **2012**, *12* (4), 278−87.
(5) Smith, M. R. *Oncogene* **2003**, *22* (47), 7359−68.
(6) Reuschenbach, M.; von Knebel Doeberitz, M.; Wentzensen, N. *Cancer Immunol. Immunother.* **2009**, *58* (10), 1535−44.
(7) Robinson, W. H.; DiGennaro, C.; Hueber, W.; Haab, B. B.; Kamachi, M.; Dean, E. J.; Fournel, S.; Fong, D.; Genovese, M. C.; de Vegvar, H. E. N.; Skriner, K.; Hirschberg, D. L.; Morris, R. I.; Muller, S.; Pruijn, G. J.; van Venrooij, W. J.; Smolen, J. S.; Brown, P. O.; Steinman, L.; Utz, P. J. *Nat. Med.* **2002**, *8* (3), 295−301.
(8) Lee, J. R.; Haddon, D. J.; Wand, H. E.; Price, J. V.; Diep, V. K.; Hall, D. A.; Petri, M.; Baechler, E. C.; Balboni, I. M.; Utz, P. J.; Wang, S. X. *Sci. Rep.* **2016**, *6*, 27623.
(9) Wang, X. J.; Yu, J. J.; Sreekumar, A.; Varambally, S.; Shen, R. L.; Giacherio, D.; Mehra, R.; Montie, J. E.; Pienta, K. J.; Sanda, M. G.; Kantoff, P. W.; Rubin, M. A.; Wei, J. T.; Ghosh, D.; Chinnaiyan, A. M. *N. Engl. J. Med.* **2005**, *353* (12), 1224−1235.
(10) Neuman de Vegvar, H. E.; Amara, R. R.; Steinman, L.; Utz, P. J.; Robinson, H. L.; Robinson, W. H. *J. Virol* **2003**, *77* (20), 11125−11138.
(11) Nakaya, H. I.; Wrammert, J.; Lee, E. K.; Racioppi, L.; Marie-Kunze, S.; Haining, W. N.; Means, A. R.; Kasturi, S. P.; Khan, N.; Li, G. M.; McCausland, M.; Kanchan, V.; Kokko, K. E.; Li, S. Z.; Elbein, R.; Mehta, A. K.; Aderem, A.; Subbarao, K.; Ahmed, R.; Pulendran, B. *Nat. Immunol.* **2011**, *12* (8), 786−795.
(12) Tran, P. H.; Peiffer, D. A.; Shin, Y.; Meek, L. M.; Brody, J. P.; Cho, K. W. Y. *Nucleic Acids Res.* **2002**, *30* (12), e54.
(13) Paweletz, C. P.; Charboneau, L.; Bichsel, V. E.; Simone, N. L.; Chen, T.; Gillespie, J. W.; Emmert-Buck, M. R.; Roth, M. J.; Petricoin, E. F., III; Liotta, L. A. *Oncogene* **2001**, *20* (16), 1981−1989.
(14) Huang, S.; Hendriks, W.; Althage, A.; Hemmi, S.; Bluethmann, H.; Kamijo, R.; Vilcek, J.; Zinkernagel, R. M.; Aguet, M. *Science* **1993**, *259* (5102), 1742−1745.
(15) Le Bon, A.; Schiavoni, G.; D'Agostino, G.; Gresser, I.; Belardelli, F.; Tough, D. F. *Immunity* **2001**, *14* (4), 461−470.
(16) Ito, K.; Smith, B. R.; Parashurama, N.; Yoon, J. K.; Song, S. Y.; Miething, C.; Mallick, P.; Lowe, S.; Gambhir, S. S. *Cancer Res.* **2012**, *72* (23), 6111−6118.
(17) Jeon, Y. H.; Choi, Y.; Kang, J. H.; Kim, C. W.; Jeong, J. M.; Lee, D. S.; Chung, J. K. *Cancer Biol. Ther.* **2007**, *6* (5), 781−786.
(18) Gaster, R. S.; Hall, D. A.; Nielsen, C. H.; Osterfeld, S. J.; Yu, H.; Mach, K. E.; Wilson, R. J.; Murmann, B.; Liao, J. C.; Gambhir, S. S.; Wang, S. X. *Nat. Med.* **2009**, *15* (11), 1327−1332.
(19) Lee, J. R.; Haddon, D. J.; Gupta, N.; Price, J. V.; Credo, G. M.; Diep, V. K.; Kim, K.; Hall, D. A.; Baechler, E. C.; Petri, M.; Varma, M.; Utz, P. J.; Wang, S. X. *ACS Nano* **2016**, *10* (12), 10652−10660.
(20) Lee, J. R.; Bechstein, D. J.; Ooi, C. C.; Patel, A.; Gaster, R. S.; Ng, E.; Gonzalez, L. C.; Wang, S. X. *Nat. Commun.* **2016**, *7*, 12220.
(21) Hall, D. A.; Gaster, R. S.; Lin, T.; Osterfeld, S. J.; Han, S.; Murmann, B.; Wang, S. X. *Biosens. Bioelectron.* **2010**, *25* (9), 2051−2057.
(22) Schmitt, C. A.; McCurrach, M. E.; de Stanchina, E.; Wallace-Brodeur, R. R.; Lowe, S. W. *Genes Dev.* **1999**, *13* (20), 2670−7.
(23) Wang, S. X.; Li, G. *IEEE Trans. Magn.* **2008**, *44* (7), 1687−1702.
(24) Gaster, R. S.; Hall, D. A.; Wang, S. X. *Lab Chip* **2011**, *11* (5), 950−956.
(25) Lee, J. R.; Sato, N.; Bechstein, D. J.; Osterfeld, S. J.; Wang, J.; Gani, A. W.; Hall, D. A.; Wang, S. X. *Sci. Rep.* **2016**, *6*, 18692.
(26) Nimmerjahn, F.; Ravetch, J. V. *Science* **2005**, *310* (5753), 1510−1512.
(27) Nimmerjahn, F.; Lux, A.; Albert, H.; Woigk, M.; Lehmann, C.; Dudziak, D.; Smith, P.; Ravetch, J. V. *Proc. Natl. Acad. Sci. U. S. A.* **2010**, *107* (45), 19396−19401.
(28) Stevens, T. L.; Bossie, A.; Sanders, V. M.; Fernandezbotran, R.; Coffman, R. L.; Mosmann, T. R.; Vitetta, E. S. *Nature* **1988**, *334* (6179), 255−258.
(29) Kalinski, P.; Moser, M. *Nat. Rev. Immunol.* **2005**, *5* (3), 251−260.
(30) Abbas, A. K.; Murphy, K. M.; Sher, A. *Nature* **1996**, *383* (6603), 787−793.
(31) Rosenberg, S. A. *Nature* **2001**, *411* (6835), 380−384.
(32) Kantoff, P. W.; Higano, C. S.; Shore, N. D.; Berger, E. R.; Small, E. J.; Penson, D. F.; Redfern, C. H.; Ferrari, A. C.; Dreicer, R.; Sims, R. B.; Xu, Y.; Frohlich, M. W.; Schellhammer, P. F.; Ahmed, T.; Amin, A.; Arseneau, J.; Barth, N.; Bernstein, G.; Bracken, B.; Burch, P.; Caggiano, V.; Chin, J.; Chodak, G.; Chu, F.; Corman, J.; Curti, B.; Dawson, N.; Deeken, J. F.; Dubernet, T.; Fishman, M.; Flanigan, R.; Gailani, F.; Garbo, L.; Gardner, T.; Gelmann, E.; George, D.; Godfrey, T.; Gomella, L.; Guerra, M.; Hall, S.; Hanson, J.; Israeli, R.; Jancis, E.; Jewett, M. A. S.; Kassabian, V.; Katz, J.; Klotz, L.; Koeneman, K.; Koh, H.; Kratzke, R.; Lance, R.; Lech, J.; Leichman, L.; Lemon, R.; Liang, J.; Libertino, J.; Lilly, M.; Malik, I.; Martin, S. E.; McCaffrey, J.; McLeod, D.; McNeel, D.; Miles, B.; Murdock, M.; Nabhan, C.; Nemunaitis, J.; Notter, D.; Pantuck, A.; Perrotte, P.; Pessis, D.; Petrylak, D.; Polikoff, J.; Pommerville, P.; Ramanathan, S.; Rarick, M.; Richards, J.; Rifkin, R.; Rohatgi, N.; Rosenbluth, R.; Santucci, R.; Sayegh, A.; Seigne, J.; Shapira, I.; Shedhadeh, N.; Shepherd, D.; Sridhar, S.; Stephenson, R.; Teigland, C.; Thaker, N.; Vacirca, J.; Villa, L.; Vogelzang, N.; Wertheim, M.; Wolff, J. H.; Wurzel, R.; Yang, C.; Young, J.; Investigators, I. S. *N. Engl. J. Med.* **2010**, *363* (5), 411−422.
(33) Zhong, L.; Coe, S. P.; Stromberg, A. J.; Khattar, N. H.; Jett, J. R.; Hirschowitz, E. A. *J. Thorac. Oncol.* **2006**, *1* (6), 513−519.
(34) Scofield, R. H. *Lancet* **2004**, *363* (9420), 1544−1546.
(35) Hueber, W.; Utz, P. J.; Steinman, L.; Robinson, W. H. *Arthritis Res.* **2002**, *4* (5), 290−295.
(36) Arbuckle, M. R.; McClain, M. T.; Rubertone, M. V.; Scofield, R. H.; Dennis, G. J.; James, J. A.; Harley, J. B. *N. Engl. J. Med.* **2003**, *349* (16), 1526−1533.
(37) Hall, D. A.; Gaster, R. S.; Makinwa, K. A. A.; Wang, S. X.; Murmann, B. *IEEE J. Solid-State Circuits* **2013**, *48* (5), 1290−1301.
(38) Lee, J. R.; Choi, J.; Shultz, T. O.; Wang, S. X. *Anal. Chem.* **2016**, *88* (15), 7457−7461.
(39) Bechstein, D. J. B.; Lee, J. R.; Ooi, C. C.; Gani, A. W.; Kim, K.; Wilson, R. J.; Wang, S. X. *Sci. Rep.* **2015**, *5*, 11693.
(40) Lin, L. W.; Pisano, A. P. *J. Microelectromech. Syst.* **1999**, *8* (1), 78−84.
(41) Sullivan, S. P.; Koutsonanos, D. G.; Del Pilar Martin, M.; Lee, J. W.; Zarnitsyn, V.; Choi, S. O.; Murthy, N.; Compans, R. W.; Skountzou, I.; Prausnitz, M. R. *Nat. Med.* **2010**, *16* (8), 915−920.
(42) Gardeniers, H. J. G. E.; Luttge, R.; Berenschot, E. J. W.; de Boer, M. J.; Yeshurun, S. Y.; Hefetz, M.; van't Oever, R.; van den Berg, A. *J. Microelectromech. Syst.* **2003**, *12* (6), 855−862.

DOI: 10.1021/acs.nanolett.7b02591
Nano Lett. 2017, 17, 6644−6652